J. Fluid Mech. (1983), *vol.* 136, *pp.* 1–30
Printed in Great Britain

Numerical experiments on Hele Shaw flow with a sharp interface

By GRÉTAR TRYGGVASON AND HASSAN AREF
Division of Engineering, Brown University, Providence, Rhode Island 02912, USA

(Received 30 March 1983 and in revised form 24 June 1983)

The fingering instability of an interface between two immiscible fluids in a Hele Shaw cell is simulated numerically. The algorithm used is based on a transcription of the equations of motion for the interface in which it formally becomes a generalized vortex sheet. The evolution of this sheet is computed using a variant of the vortex-in-cell method. The resulting scheme and code make it possible to follow the collective behaviour of many competing and interacting fingers well into the nonlinear, large-amplitude regime. It is shown that in this regime the evolution is controlled essentially by just one dimensionless parameter, the ratio of fluid viscosities. The effects of varying this parameter are studied and the results compared with experimental investigations. Scaling properties of the average density profile across the evolving mixed layer between the two homogeneous fluid phases are investigated. Many phenomena are observed that must be characterized as collective interactions and thus cannot be understood in terms of flows with just a single finger.

1. Introduction

Sharp interfaces, both stable and unstable, in unsteady motion occur frequently in fluid mechanics. For an unstable situation small changes in the initial state may amplify rapidly to produce completely different details in interfacial structure at later times. For brevity we shall refer to such behaviour as 'chaotic'. Indeed, only certain average properties of an interface may be reproducible in an experiment. Again, an interface between two fluids, along which there is essentially no diffusion, may evolve in such a way that substantial entrainment and mixing occurs. Both these possibilities, viz a 'chaotic' system with efficient macroscopic (as opposed to 'molecular') mixing, are familiar from conventional turbulent flows.

The equations describing interfaces are generally nonlinear. Furthermore, interfaces are usually three-dimensional and can be difficult to visualize and hence to study both experimentally and numerically. Analytical investigations of the governing nonlinear equations must usually be content with stability considerations for very regular configurations, such as flat, circular or spherical interfaces, and to the limit of small-amplitude disturbances.

A relatively simple example of the above type, which, however, still contains many ingredients of more complicated systems, is the interface between two immiscible fluids in a Hele Shaw cell (Hele Shaw 1898), the celebrated Taylor–Saffman instability (Saffman & Taylor 1958). This system is two-dimensional by construction, and it is therefore more accessible to numerical calculations. Usually two-dimensionality must be enforced by neglecting three-dimensional effects with a consequent loss of realism and relevance. In addition, the Taylor–Saffman instability has considerable importance for various technological endeavours.

The initial motivation in the 1950s to study this instability came from the analogy between Hele Shaw flow and flow in a two-dimensional slab of porous medium (see Todd 1955). It was observed that, if water was used to drive out residual oil from the porous rock in an oilfield, a considerable amount of oil was left in the ground when water appeared at the producing wells. This disappointing result is believed to be in part due to a fingering instability of the oil–water interface. Because of its great economic importance, oil–water flow in porous media has been the subject of intensive study in the petroleum–engineering literature (see Perkins, Johnston & Hoffmann (1965) and other articles in the same journal). These studies have been primarily experimental, and their main purpose has been to develop engineering correlations for application to a real field situation. Some of the experiments were performed in three-dimensional packed-bed models (see e.g. the beautiful pictures of a transparent model due to van Meurs 1958), but others employed the Hele Shaw cell.

Fingering in porous media also occurs during gas injection, as used in the underground storage of gas, and in water infiltration (Wooding & Morel-Seytoux 1976). The Hele Shaw fingering mechanism is also thought to be relevant by analogy to the form and growth of fingered sheet intrusions in geological formations (Pollard, Muller & Dockstader 1975) and to the problem of dendritic growth (Langer 1980). The Hele Shaw equations are similar to the ones used to describe the deformation of ionospheric plasma clouds (Overman, Zabusky & Ossakow 1983). For a general review of two-phase flow in porous media including fingering see Wooding & Morel-Seytoux (1976).

Although the applicability of results for fingering in a Hele Shaw cell to flow under actual reservoir conditions, where the flow is three-dimensional and 'dispersion' of the interface can occur, is not unquestionable (Wooding & Morel-Seytoux 1976), it is to be expected that an investigation of this problem will be helpful to the understanding of many general properties of unsteady interface motion. We share the view of Langer (1980) that in order to understand interfacial instability in general a 'detailed analysis of experimentally realizable, physical systems' is necessary. Another reason for choosing to study Hele Shaw flow is that we have developed a useful code for the numerical computation of this type of interface. Thus portions of this paper are of interest from a purely methodological point of view. The use of the Hele Shaw equations as a model problem for numerical calculation of two-dimensional, transient, free boundary problems has previously been stressed by Meyer (1981).

The discussion of interfaces in a Hele Shaw cell is commonly divided into the two cases of miscible and immiscible fluids. For immiscible fluids there is a finite surface tension that stabilizes small-scale disturbances. For miscible fluids the interdiffusion of the fluids has a stabilizing effect. If the velocity of interfacial fingers is much higher than the characteristic diffusion velocity, diffusion will not affect the initial shape of the fingers, and they should be similar to those of the immiscible case. For a discussion of this effect in a packed bed model see Slobod & Thomas (1963). Here we consider only immiscible fluids (since that is the case we are capable of calculating numerically), but for the reasons just mentioned we believe that some of our conclusions are valid for miscible fluids as well.

An interface in a Hele Shaw cell can be unstable for two reasons. If a heavier fluid is on top of a lighter one, the interface is gravitationally unstable. If, owing to pumping, a less viscous fluid is made to displace a more viscous one, the interface is also unstable. These two effects can occur simultaneously, and for the equations

used here it will be shown that they are interchangeable. This, of course, need not be so in general, and we shall discuss a modification of the equations where this is not the case.

One of the first experimental demonstrations of unstable fingering in a Hele Shaw cell is due to Saffman & Taylor (1958). They performed a linear stability analysis of the flat interface, neglecting surface tension, and found an analytic solution for the shape of the single fingers that represented the late stages of their experiments. A stability analysis including surface tension was performed by Chuoke, van Meurs & van der Poel (1959) who also performed experiments both in packed bed models and in a Hele Shaw cell. The Saffman–Taylor experiment has since been repeated by several investigators (see e.g. Gupta, Varnon & Greenkorn 1973; Pitts 1980). Paterson (1981) has recently investigated radial fingering using immiscible fluids. Rosensweig (1982) shows fingering instabilities leading to some remarkable equilibrium patterns for ferrofluid in a Hele Shaw cell with forcing by a combination of gravity and a gradient of magnetic field. Experiments involving miscible fluids have also been performed. Many of the experiments done by researchers primarily interested in secondary oil recovery employed miscible fluids, since this situation was considered more relevant to actual reservoir conditions. Of particular interest are the experiments performed by Wooding (1969), in which miscible oils with rather similar viscosities but different densities in a gravitationally unstable Hele Shaw flow are used. The final stages in this experiment consist of many long fingers, and the strong suppression of small fingers seen in the Saffman–Taylor experiment is not observed. These fingers also have a shape different from that of the single Saffman–Taylor finger. Wooding's mixed layer is, furthermore, (more or less) up–down symmetric about the initial position of the interface. These differences between the Wooding experiment and the Saffman & Taylor experiment are largely due to the difference in the viscosity contrast between the two fluids, as we shall demonstrate later.

The remainder of our paper is set out as follows. In §2 we discuss the Hele Shaw equations, and, for the case of a single interface between two immiscible fluids, cast the problem in terms of the evolution of a vortex sheet. Here we are following the work of de Josselin de Jong (1960), but, whereas he simply stated what amounts to an algorithm for following interface motion, we present both a comprehensive restatement and an implementation. We shall see that the Hele Shaw problem is more complicated than the evolution of a simple vortex sheet in two-dimensional, inviscid, incompressible flow, because the circulation is constantly changing, but less complicated than the two-dimensional Rayleigh–Taylor problem with sharp stratification (Birkhoff 1954; Baker, Meiron & Orszag 1980). The vortex-sheet strength for Hele Shaw flow is given by an integral equation, whereas for the Rayleigh–Taylor problem one must solve an auxiliary integrodifferential equation. Various formal observations on rescaling the equations of motion are made. In §2 we also discuss the numerical scheme used to implement the algorithm. We have chosen to follow the temporal evolution of the interface using the vortex-in-cell scheme described a decade ago by Christiansen (1973). This allows us to compute interfaces that have many competing fingers, although possibly with some sacrifice of numerical accuracy of very-small-scale effects. Section 2 contains a thorough discussion of such methodological points.

Section 3 presents our results. We have systematically investigated the nature of the interface geometry (starting from a predetermined initial disturbance) as the governing non-dimensional parameters are varied. The differences observed experimentally by Saffman & Taylor and by Wooding can now be rationalized. We observe various secondary phenomena known from other systems, such as growth and

merging of large-scale structures, and, to a lesser extent, the tearing apart of structures. The differences in the degree to which these phenomena develop as we increase the viscosity contrast across the interface is elucidated. Section 3 concludes with a discussion of various averaged quantities that indicate scaling with the width of the mixed layer.

In §4 we discuss and summarize our results and mention some possible extensions. Modifications of our model equations to include certain effects of experimental significance are also discussed.

A short account of the work reported here was presented at the American Physical Society, Division of Fluid Dynamics annual meeting at Rutgers University (Aref & Tryggvason 1982). A more complete presentation was given as part of the Workshop on Instability Modelling and Front Tracking at Los Alamos National Laboratory (1–4 February 1983). A brief review of the present work and discussion of some extensions appears in Aref & Tryggvason (1984).

2. The numerical algorithm and its implementation

Frequently in fluid dynamics most of the flow field can be considered irrotational and the vorticity non-zero only in some region of finite extent. In several cases of interest the rotational domain is very thin in one direction, and it is a useful idealization to neglect its thickness altogether and to model the region of non-zero vorticity as a vortex sheet.

In two dimensions the velocity field $\boldsymbol{u}(\boldsymbol{x},t)$ due to a vortex sheet parameterized through $\boldsymbol{x}'(s,t)$ is then given by the integral formula (Batchelor 1967)

$$\boldsymbol{u}(\boldsymbol{x},t) = \frac{1}{2\pi}\int \frac{\hat{\boldsymbol{z}}\times(\boldsymbol{x}-\boldsymbol{x}'(s,t))}{|\boldsymbol{x}-\boldsymbol{x}'(s,t)|^2}\,\gamma(s,t)\,\mathrm{d}s, \tag{1}$$

where s is arclength, $\gamma(s,t)$ is the vortex-sheet strength and $\hat{\boldsymbol{z}}$ is a unit vector perpendicular to the plane of motion. For inviscid fluid of constant density the circulation around any material curve is constant according to Kelvin's theorem (see Lamb 1932), so the only changes in the vortex-sheet strength arise from the stretching of the sheet. If a two-dimensional vortex sheet is modelled as a row of point vortices, the situation is particularly simple: each elemental vortex retains its initial circulation. This simplicity of the point-vortex model has attracted many investigators, starting with Rosenhand's (1931) hand calculations of the roll-up of a vortex sheet. For review and discussion the reader is referred to Leonard (1980), Moore (1981) and Aref (1983). When the fluid is not of constant density, but can still be considered inviscid, Kelvin's theorem is replaced by Bjerknes' law (Prandtl & Tietjens 1934), and vorticity is generated as a consequence of the inclination between gradients of pressure and density. Again, if the change in density takes place in a thin layer, its thickness may be ignored and the layer modelled as a vortex sheet. The equations for the vortex-sheet strength now become more complicated integral or integrodifferential equations. This model has, nevertheless, also been the subject of extensive study, both for stably stratified fluid (waves) and for unstably stratified fluid (Rayleigh–Taylor instability). Early work on the basic formulation and algorithm is due to Birkhoff (1954). Recent implementations for the unstable problem may be found in Baker *et al.* (1980) and for the problem of waves in Longuet-Higgins & Cokelet (1976) and in Baker, Meiron & Orszag (1982).

The flow of inviscid fluid with piecewise constant density is not the only system that can be calculated by tracking the motion of a vortex sheet. As was pointed out

by de Josselin de Jong (1960), the interface between fluids with different but constant material properties (density and viscosity) in a porous medium can also be modelled as a vortex sheet, when the fluids move according to Darcy's law (Bear 1972). The only implementation known to us of this method is the calculation by Meng & Thomson (1978). However, that calculation is applicable only to the case of weak viscosity stratification.

Consider then a vortex-sheet interface discretized into point-vortex elements. To find the velocity of each point vortex it is in principle necessary to sum over all the others, and the number of operations per time step will therefore be $O(N^2)$, where N is the number of vortices. For a highly distorted interface a large number of point vortices is required and computations using (1) and summing interactions pairwise become impracticable. However, a different approach is possible. The stream function ψ corresponding to the velocity field in eqn. (1) satisfies a Poisson equation

$$\Delta\psi = -\omega, \tag{2}$$

where ω is the (singular) vorticity distribution. For the case of a highly contorted interface it may be more economical to solve this elliptic field equation directly on an underlying grid. For domains of regular shape, such as a rectangle, 'fast' Poisson-equation solvers are available. These make the number of operations required to find the stream function, and hence the velocity field, proportional to $M^2 \ln M$ (at worst), where M is the number of grid points in one direction. Since the spatial resolution is cut off at some fraction of a grid spacing, it is sufficient to have approximately one vortex per grid square. Thus, for a highly distorted interface (or for several interfaces) N can be taken proportional to M^2 and the operation count becomes $O(N \ln N)$ per time step as compared with $O(N^2)$ for direct summation schemes. This represents a significant reduction in required computer time. For an almost straight interface there will be no reduction since N will then be proportional to M (not M^2) and the operation count will actually go up by a factor $\ln M$. The method described (and the argument given here) is a straightforward extension of the so-called vortex-in-cell algorithm introduced by Christiansen (1973) for homogeneous two-dimensional flows. As mentioned previously, it was first used by Meng & Thomson (1978) for the case of a small jump in fluid viscosity across the interface. Here the method is extended to and implemented for arbitrary stratification.

2.1. *Basic equations for stratified Hele Shaw flow*

The equations conventionally used to describe flow in a Hele Shaw cell are (Lamb 1932; Bear 1972)

$$\nabla p = -(12\mu/b^2)\,\boldsymbol{u} - g\rho\hat{\boldsymbol{j}}, \tag{3}$$

$$\nabla \cdot \boldsymbol{u} = 0. \tag{4}$$

In these equations μ is the fluid viscosity, b is the spacing between the plates in the Hele Shaw cell, ρ is the fluid density, g the acceleration due to gravity, and $\hat{\mathbf{j}}$ is a unit vector directed upward (see figure 1). The velocity vector $\boldsymbol{u}$ has just two components dependent on time and on the coordinates x, y in the plane of the Hele Shaw cell. The two-dimensional field $\mathbf{u}$ arises by taking an average of the full three-dimensional flow field that describes the penetration of the fluid into the narrow space between the plates in the Hele Shaw cell. This procedure is explained in detail by Bear (1972). The quantity p in (3) is a similarly averaged pressure. Since the solutions to these equations will not in general satisfy the no-slip boundary condition at the sides of the Hele Shaw cell, an independent singular perturbation analysis is called for in these

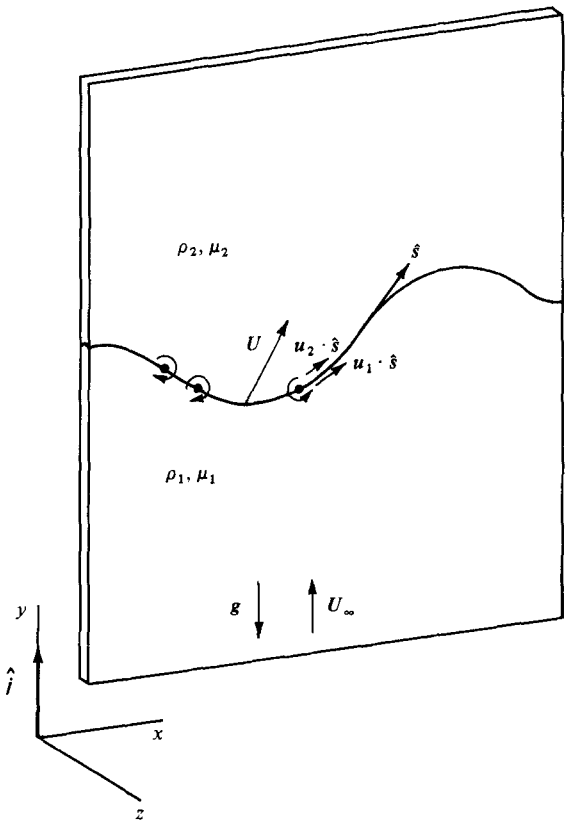

FIGURE 1. Sketch defining the notation used. Fluids are labelled 1 (below) and 2 (above) the interface.

regions. Such an investigation has been performed by Rigels (1938) and Thompson (1968) (see also the short discussion by Lamb 1932). We shall sidestep this problem by doing our calculations in a box with periodic boundary conditions in the x-direction (see figure 1), and no through-flow conditions at the boundaries above and below the interface. We have taken care to keep these boundaries sufficiently far from the interface so that its evolution is not disturbed by their existence. At the interface itself there must in reality also be a three-dimensional boundary layer, but following other workers we assume its thickness to be negligible. Later, when we come to discuss the experimental results that are available in the literature, we shall have additional comments on the applicability of (3) and (4) to a real Hele Shaw apparatus.

We shall now derive the essential formulae for the vortex sheet representation of a stratified flow in a Hele Shaw cell. Let the space between the plates be occupied by a system of two immiscible fluids labelled 1 and 2 (see figure 1). The fluids meet at an interface idealized as a plane curve with unit tangent $\hat{\boldsymbol{s}}$. It is really not essential that there be just one interface or that it be simply connected, but for convenience we shall think in terms of such a situation. The normal component of the velocity across the interface must be continuous because of (4) and equal to the normal component of the velocity of propagation of the interface itself. The tangential component of the velocity, however, is discontinuous and gives rise to the vortex sheet strength γ defined by

$$\gamma = (\boldsymbol{u}_1 - \boldsymbol{u}_2) \cdot \hat{\boldsymbol{s}}, \tag{5}$$

where $\boldsymbol{u}_1$ ($\boldsymbol{u}_2$) is the velocity just below (above) the interface. An equation for γ is easily obtained by taking the dot product of (3) with the tangent vector both in fluid 1 and in fluid 2 and then subtracting one from the other:

$$(\nabla p_2 - \nabla p_1)\cdot\hat{\boldsymbol{s}} = -\left(\frac{12\mu_2}{b^2}\boldsymbol{u}_2 - \frac{12\mu_1}{b^2}\boldsymbol{u}_1\right)\cdot\hat{\boldsymbol{s}} - g(\rho_2-\rho_1)\hat{\boldsymbol{j}}\cdot\hat{\boldsymbol{s}}. \tag{6}$$

Rewriting this slightly, using (5) and the abbreviations $\Delta p = p_2 - p_1$, $\Delta\rho = \rho_2 - \rho_1$, $\Delta\mu = \mu_2 - \mu_1$, $\bar{\mu} = \frac{1}{2}(\mu_2+\mu_1)$ and $\boldsymbol{U} = \frac{1}{2}(\boldsymbol{u}_1+\boldsymbol{u}_2)$, we obtain

$$\gamma = \frac{\Delta\mu}{\bar{\mu}}\boldsymbol{U}\cdot\hat{\boldsymbol{s}} + \frac{b^2 g}{12\bar{\mu}}\Delta\rho\hat{\boldsymbol{j}}\cdot\hat{\boldsymbol{s}} + \frac{b^2}{12\bar{\mu}}\nabla(\Delta p)\cdot\hat{\boldsymbol{s}}. \tag{7}$$

Here the subscript 1 (2) means the value as the interface is approached from below (above). The third term on the right will either vanish or be given in terms of the surface tension as we shall discuss shortly. From (1) the sheet velocity $\boldsymbol{U}$ is related to γ by Birkhoff's (1954) integral formula

$$\boldsymbol{U} = \boldsymbol{U}(s,t) = \frac{1}{2\pi}\,\mathrm{P}\int \frac{\hat{\boldsymbol{z}}\times(\boldsymbol{x}(s,t)-\boldsymbol{x}(s',t))}{|\boldsymbol{x}(s,t)-\boldsymbol{x}(s',t)|^2}\,\gamma(s',t)\,\mathrm{d}s', \tag{8}$$

where the principal-value integral is taken along the sheet. Note that, because of (8), (7) is an integral equation for γ. As we have already mentioned, for the Rayleigh–Taylor problem one obtains an integrodifferential equation for γ. This difference results from the total absence of convective acceleration (or 'inertia') terms in the Hele Shaw equations.

When the interface is modelled as a row of point-vortex elements the circulation of the vortex at arclength s_i is

$$\Gamma_i = \gamma(s_i)\,\Delta s, \tag{9}$$

where Δs is the spacing between vortices. The z-component of vorticity is then

$$\omega(\boldsymbol{x},t) = \Sigma\,\Gamma_i\,\delta(\boldsymbol{x}-\boldsymbol{x}_i(t)), \tag{10}$$

where $\boldsymbol{x}_i$ is the position vector of elemental vortex i. To compute the time evolution of the interface we calculate the sheet velocity from (8) and move vortex i according to

$$\mathrm{d}\boldsymbol{x}_i/\mathrm{d}t = \boldsymbol{U}(s_i). \tag{11}$$

Once moved, we iterate (7) with $\boldsymbol{U}$ given in principle by (8), using the new sheet position, until convergence is obtained. Then we reassign vortex circulations. In practice vortex velocities are not found by computing (8) as it stands but rather by the vortex-in-cell scheme as we have already explained.

To specify the problem completely, it remains to relate the difference in pressure gradients in (7) to other properties. The simplest assumption is that the pressures are the same on both sides of the interface, so that the last term would be identically zero (this implies that there is no surface tension at the interface). For stably stratified flow this might not be a bad assumption, but for unstable stratification it is physically unreasonable, and leads to numerical difficulties for the following reasons. It is found from linear stability analysis that, when the last term in (7) vanishes, the growth rate of a small disturbance is proportional to the wavenumber. Thus a disturbance of arbitrarily short wavelength will grow arbitrarily fast. In numerical calculations, however, one can, in general, only attain a finite spatial resolution. Hence modes with wavelengths shorter than the smallest scales resolved are misrepresented. If these modes have the fastest time dependence, serious errors may result. In effect the cutoff provided by the finite spatial resolution acts as a damping on the smallest scales. This damping may or may not be physically plausible.

By neglecting the viscous stresses at a moving interface in a real Hele Shaw cell, we can write the pressure drop approximately as

$$p_2 - p_1 = \alpha\left(\frac{1}{R_\parallel} + \frac{1}{R_\perp}\right), \tag{12}$$

where α is the surface-tension coefficient, $R_\parallel$ is the radius of curvature of the interface in the plane of motion (the (x, y)-plane, see figure 1) and $R_\perp$ is the radius of curvature in the direction perpendicular to the parallel plates. We shall follow other workers (McLean & Saffman 1981) and assume that $R_\perp$ is constant. Then we get simply (cf. (7))

$$\nabla(\Delta p)) \cdot \hat{\boldsymbol{s}} = \alpha \frac{\partial}{\partial s}\left(\frac{1}{R_\parallel}\right). \tag{13}$$

It is not at all obvious that this is a permissible assumption. We shall discuss it in more detail later. For flow in a porous medium the conditions at the interface are probably very different and more complicated owing to the dispersive nature of the medium. Early workers in oil–water flow (e.g. Richardson 1961) found it useful to define an effective surface tension, which was usually considerably larger than the surface tension for the same fluids when brought into contact outside the porous medium.

In general the interface will be moving in some irrotational flow field $\boldsymbol{U}_{\rm pot}$ caused by the boundary conditions, or by a distribution of sources and sinks inside the domain under study. The velocity of the interface can then be separated into two parts $\boldsymbol{U}_{\rm tot} = \boldsymbol{U} + \boldsymbol{U}_{\rm pot}$, where $\boldsymbol{U}$ is the velocity induced by the vortex sheet (equation (8)). In the calculations described here the irrotational velocity field will consist of a uniform velocity $U_\infty \hat{\boldsymbol{j}}$, although the algorithm could easily accommodate a more general irrotational flow. In (11) we must now use $\boldsymbol{U}_{\rm tot}$ on the right-hand side. However, we shall make use of a frame of reference moving with velocity $U_\infty \hat{\boldsymbol{j}}$. As we shall see below, U_∞ really only enters the problem if we need the true position of the interface in the 'laboratory' frame of reference. With U_∞ added, (7) becomes

$$\gamma = \frac{\Delta\mu}{\bar{\mu}}\, \boldsymbol{U} \cdot \hat{\boldsymbol{s}} + \left(\frac{\Delta\mu}{\bar{\mu}} U_\infty + \frac{\Delta\rho g b^2}{12\bar{\mu}}\right) \hat{\boldsymbol{j}} \cdot \hat{\boldsymbol{s}} + \frac{\alpha b^2}{12\bar{\mu}} \frac{\partial}{\partial s}\left(\frac{1}{R_\parallel}\right), \tag{14}$$

where we have used (13). The coefficient of $\hat{\boldsymbol{j}} \cdot \hat{\boldsymbol{s}}$ has the dimensions of velocity, so, in order to non-dimensionalize the equations, we define a speed U_* to be the absolute value of this constant coefficient:

$$U_* = \left| \frac{(\mu_2 - \mu_1)\, U_\infty + \frac{1}{12}(\rho_2 - \rho_1)\, g b^2}{\mu_2 + \mu_1} \right|. \tag{15}$$

In order to reduce the number of variable parameters in the problem, we now proceed to obtain a non-dimensional form of (14). We shall non-dimensionalize lengths in two different ways, each corresponding to different flow regimes. First, we assume that there exists some characteristic external length W which has a significant influence on the problem. Then W is a natural choice in non-dimensionalizing lengths. For an experimental setup of the type usually considered in the literature, the width of the cell is a natural choice for W. For numerical simulations using periodic boundary conditions, W can be taken as the period, although it does not completely correspond to rigid walls. With this choice of lengthscale we proceed as follows. Let $s = \tilde{s} W$, $\boldsymbol{U} = \tilde{\boldsymbol{U}} U_*$, $R_\parallel = \tilde{R}_\parallel W$ and $\gamma = \tilde{\gamma} U_*$. Dividing (14) by U_*, we obtain an

equation for the non-dimensional vortex-sheet strength $\tilde{\gamma}$:

$$\tilde{\gamma} = 2A(\tilde{\boldsymbol{U}} \cdot \hat{\boldsymbol{s}}) \pm 2\hat{\boldsymbol{j}} \cdot \hat{\boldsymbol{s}} + 2B \frac{\partial}{\partial s}\left(\frac{1}{\tilde{R}_{\parallel}}\right). \tag{16}$$

In this equation, which in view of (8) is an integral equation for $\tilde{\gamma}$,

$$A = \frac{\mu_2 - \mu_1}{\mu_2 + \mu_1} \tag{17}$$

is a viscosity 'Atwood ratio'† and

$$B = \frac{\alpha b^2}{12 U_* W^2 \bar{\mu}} \tag{18}$$

is a non-dimensional surface-tension coefficient. It can be interpreted as the ratio of the surface-tension force to the driving force, and for gravity-driven instability reduces to the inverse of the ordinary Bond number.

This form of the equation reveals many interesting properties of the flow. First of all, the quantity U_* sets the timescale of the motion. The non-dimensional time $\tilde{t} = U_* t/W$. It can also be shown that for vanishing surface tension the sign of the quantity inside the absolute-value sign in (15) determines the stability of an initially flat interface to infinitesimal disturbances (Saffman & Taylor 1958). The viscosity difference multiplied by the initial velocity of the sheet and/or the density difference times the acceleration of gravity is the force (per unit volume) that causes small disturbances to either grow or be damped out. Note that, since the same combination appears in B, $\Delta\mu U_\infty$ can be replaced by $\frac{1}{12}\Delta\rho g b^2$ without affecting the equations. That is, according to (3) and (4) and the jump condition (13), a horizontal Hele Shaw cell with throughflow U_∞ is equivalent to a vertical Hele Shaw cell with density stratification, so long as the boundary effects can be ignored. It should be pointed out that in a real experiment, where Δp might depend on the velocity of propagation of the interface (Dussan V. 1979), this is not necessarily true (see also § 4). The coefficient A (equation (17)) determines the influence of the induced velocities on the vortex-sheet strength. For $A = 0$ (no viscosity difference) there is no 'feedback' from the velocities, and it may be shown that for disturbances that have initial 'up–down' symmetry the interface will retain this discrete symmetry for all time. (For $U_\infty \neq 0$ we must consider a coordinate system moving with veocity U_∞ for this statement to be valid.) The case $A = 0$ is of course slightly unphysical, since we are postulating no difference in viscosity for a case where there is a difference in density. (One can obviously only achieve this limit by working with a gravitationally driven cell.) It is formally a very convenient limit, however, since, as we have just mentioned, (16) reduces from an integral equation to a simple algebraic relation. For $A \neq 0$ the interface no longer stays up–down symmetrical, with the tendency to asymmetry becoming increasingly pronounced as $A \to \pm 1$. It can also be seen that A and $-A$ lead to interfaces that are mirror images of one another. Therefore, when exploring solutions of these equations, it is sufficient to consider the range $0 \leqslant A \leqslant 1$.

The role of the surface tension coefficient B is best seen by using the result from linear stability analysis (Saffman & Taylor 1958; Chouke *et al.* 1959) that the non-dimensional growth rate $\tilde{\sigma}$ of a small-amplitude wave is given by

$$\tilde{\sigma} = 2\pi\tilde{k}(1 - B(2\pi\tilde{k})^2), \tag{19}$$

with $\tilde{k}$ a non-dimensional wavenumber, $k = \tilde{k}W$, where k is the physical wavenumber.

† The petroleum engineer may prefer the 'mobility ratio' μ_1/μ_2 to A. Clearly these are in a one-to-one correspondence.

From this it is obvious that there is a wavenumber cutoff at

$$\tilde{k}_c = 1/2\pi B^{\frac{1}{2}},$$

and a maximum growth rate occurs at

$$\tilde{k}_{max} = \sqrt{\tfrac{1}{3}}\,\tilde{k}_c.$$

It is interesting to note that A does not appear in this expression. The term proportional to A in (16) is a second-order effect in the (small) amplitude, which, however, has considerable effect at finite amplitudes. With no surface tension there is not only no cutoff wavenumber; there is no natural lengthscale in the problem at all.

In numerical simulations the discretization imposes a limitation on the range of scales that can be resolved. If the vortex sheet is modelled as a row of point vortices, the non-dimensional growth rate of a small disturbance to an initially straight interface is given by

$$\tilde{\sigma} = 2\pi\tilde{k}(1 - B(2\pi\tilde{k})^2)\left(1 - \frac{2\tilde{k}}{N}\right), \tag{20}$$

where N is the total number of vortices in $\tilde{k}$ waves. For B equal to zero there is now still a cutoff wavenumber $\tilde{k}_c = \frac{1}{2}N$ and a wavenumber $\tilde{k}_{max} = \frac{1}{4}N$, corresponding to the fastest-growing wave (cf. Birkhoff 1954). In point-vortex simulations of vortex sheets it is therefore essential to choose B such that the effects of this 'numerical surface tension' are minimized.

The above non-dimensional form (16) is obviously always valid, and is very convenient for numerical simulations, since one can always work with a domain of width unity. However, sometimes a different choice of the lengthscale W is possible, and in some sense more appropriate. When the length of the period, or the width of the cell, is much larger than the most-unstable wavelength, it seems reasonable to assume that the development of a disturbance is not affected by this length. Assuming no external lengthscale, the independent variables of the problem are the arclength s on the interface and the time t. The parameters in the equations are U_*, $\alpha b^2/\bar{\mu}$ (and, of course, A). This suggests the scaling

$$s' = sU_*^{\frac{1}{2}}\left(\frac{\bar{\mu}}{\alpha b^2}\right)^{\frac{1}{2}}, \quad t' = tU_*^{\frac{3}{2}}\left(\frac{\bar{\mu}}{\alpha b^2}\right)^{\frac{1}{2}},$$

where the prime denotes the non-dimensional variables. If $\tilde{s}$ and $\tilde{t}$ denote the non-dimensional variables as scaled previously (i.e. using the external lengthscale W) then we have:

$$s' = \frac{\tilde{s}}{B^{\frac{1}{2}}}, \quad t' = \frac{\tilde{t}}{B^{\frac{1}{2}}}.$$

Our equations are now easily rewritten in terms of the variables s', t' by simply setting B equal to unity in the equations written in terms of $\tilde{s}$, $\tilde{t}$. Since B, or the surface tension, can be scaled out in this way, and we have assumed that external lengthscales are unimportant, it follows that various properties of the flow field must be independent of the surface tension. In particular, if the interface develops into an asymptotic state where the ratio of the width of a finger of one fluid to the width of fingers of the other fluid is some constant, then the value of this constant must be independent of surface tension. Our interest is primarily in interface motion where this scaling is valid, and the only parameter is the viscosity ratio A.

In their investigation of the effects of surface tension on a single finger, McLean & Saffman (1981) found the ratio of finger width to channel width to decrease with

decreasing surface tension. Their single-finger solutions do not belong to the regime where our scaling is valid. Note that imposing periodic boundary conditions is not by itself enough to remove the effects of an external lengthscale. For large surface tension (or B) the interface can be stable, and the period itself provides an external lengthscale. We shall return in §3.2 to the evidence that we have accumulated indicating a regime of 'statistical fingering' in which the geometry of the interface is independent of surface tension.

2.2. *Numerical considerations*

The numerical code used is an elaboration of the vortex-in-cell code described earlier by Aref & Siggia (1980, 1981). Most of the numerical calculations were performed on the CRAY-1 computer at the National Center for Atmospheric Research. The original code was written for inviscid constant-density fluid, so the circulation of each vortex was kept constant. Here that is no longer true, as we have explained, and the circulation of each point vortex must be updated at every time step. A finite-difference approximation to the equation (16) for the circulation is (cf. (9))

$$\Gamma = 2(A(u\Delta x + v\Delta y) \pm \Delta y + B\Delta(1/R_{\|})). \tag{21}$$

Here the $-$ $(+)$ sign refers to (un)stable stratification. We have written $\boldsymbol{U}\cdot\hat{\boldsymbol{s}}$ as $(u\Delta x + v\Delta y)/\Delta s$, where Δx (Δy) is the change in x (y) coordinate over an increment of arclength Δs. Similarly, $\Delta(1/R_{\|})$ is the change in $1/R_{\|}$ over arclength Δs.

For $A = 0$ it is a simple matter to update the circulations, but for non-zero A an iterative procedure is necessary. The circulation is first calculated using the velocities at the previous position (taken as zero initially). Once new velocities have been found the circulation is updated and this is continued iteratively until the values of the velocities converge. The predictor–corrector scheme used for the time stepping (Shampine & Gordon 1975) requires the evaluation of the velocities twice per time step using in both cases the above iteration. This iteration is similar to the one used by Baker *et al.* (1980). For sufficiently smooth interfaces the iteration converges very rapidly (2–4 iterations), but for a strongly deformed interface (and a value of A close to unity) the number of iterations required increases dramatically (to more than 20). In some cases, particularly for closed contours ('bubbles') it was found that the use of a relaxation parameter (equal to 0.5) greatly reduced the number of iterations needed, but for other configurations this saving was not experienced. A systematic search for an optimum way of using a relaxation parameter has not been performed, but it is plausible that significant improvements can be achieved by pursuing such a search. Another way to reduce the number of iterations is to improve the first guess of the values of the velocities by not simply taking them equal to the values at the last positions. An accelerated iteration of this type is used in Baker *et al.* (1982).

As the vortex sheet moves, it is stretched unevenly along its length. Somewhere the vortices will be far apart, elsewhere they will become clustered together. Since the representation by a row of discrete vortices introduces a stabilizing effect, somewhat like surface tension, as discussed above (see also Birkhoff 1954), a few vortices on a stretched part of the curve may lead to high apparent surface tension, as well as poor representation of that part of the interface. Therefore, it is necessary to redistribute the vortices evenly along the interface at every time step (for a discussion of the effect of redistributing see also Moore 1981). In the redistributing scheme adopted here, the interface is assumed to consist of straight-line segments between the points (a polygon line). The total length is calculated first, and then the points are redistributed onto the polygon. This rather crude redistributing scheme

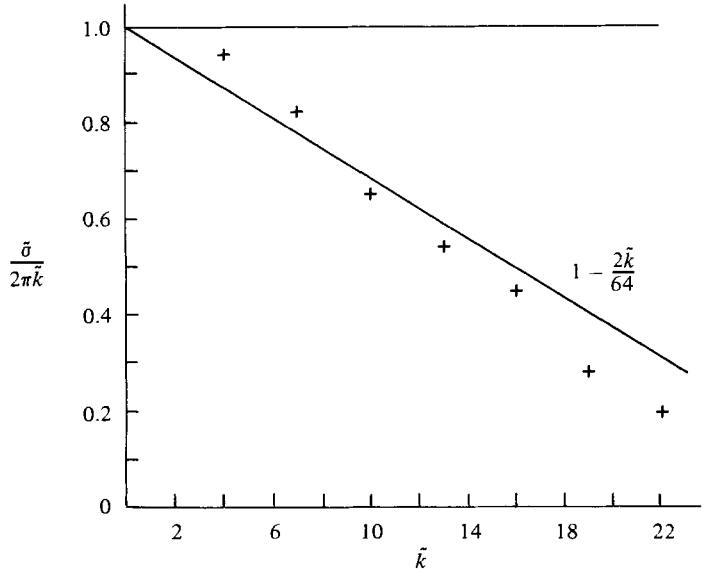

FIGURE 2. Non-dimensional growth rate $\tilde{\sigma}$ of a small-amplitude wave for $A = B = 0$. The prediction of linear stability theory is $\tilde{\sigma}/2\pi\tilde{k} = 1$, where $\tilde{k}$ is the non-dimensional wavenumber. The line $\tilde{\sigma}/2\pi\tilde{k} = 1 - 2\tilde{k}/64$ is the predicted result for an interface modelled as a row of vortices, 64 per unit length. The growth rate calculated using a 64^2 grid and 1024 particles is shown by +.

was considered to be sufficiently accurate, since in practice the distance between points is usually much less than a grid spacing, and the error introduced by redistributing is expected to be small compared with the errors introdued by the vortex-in-cell grid. The updating of the vortex strengths, the iteration when $A \neq 0$ and the redistributing constitute the main additions that were made to the original vortex-in-cell code for the calculations performed here. In the calculations of Aref & Siggia (1980, 1981) it was argued and checked that small-scale behaviour did not influence the configuration of large-scale vortex regions. Hence, in those calculations it was considered legitimate to allow the initial vortex sheet to break up. Here, since we are modelling a physical interface and similar vorticity concentration does not occur, this would not be permissible, and a continous curve must be maintained at all times.

In order to gain some understanding of the limitations of the code it was tested in various ways. From linear stability analysis it is seen that the error in the growth rate of a disturbance to an initially flat interface is of order Δx when a direct summation of vortex interactions is used (cf. (20)). Here $\Delta x = W/N$ is the distance between neighbouring vortices. When the velocities are calculated on a grid, the grid spacing determines the resolution. The growth rate of a small wave was calculated on a 64^2 grid for various wavenumbers and $B = 0$. In figure 2 this growth rate is compared with the growth rate for the direct-summation method as predicted by linear stability analysis. The number of vortices was many times the number of grid spaces. It is seen from the figure that as far as predicting the growth rate of an initially flat interface is concerned the vortex-in-cell scheme is comparable to the direct summation method. Its advantage is of course the computational economy for highly contorted interfaces. The 'smearing out' of the vorticity onto the grid gives the vortex sheet a finite thickness of about one grid spacing. Thus, when the wavelength of a

disturbance is comparable to a grid spacing, it will 'feel' the stabilizing effect of this thickness. For low wavenumbers the results are actually better than those obtained by direct summation. This might be due to the anisotropy of the velocity field with respect to the grid (Aref & Siggia 1980) or to small-scale disturbances introduced by the grid which are growing faster than the initial wave.

In order to investigate the effects of numerical errors on the performance of a computer code, it is common to run the results of an initial-value problem backwards to test for 'reversibility'. In our case this is not possible for the following reason. When the code is run forward it is necessary to use non-zero surface tension to stabilize small disturbances. When the code is run backwards, the previously unstable long-wavelength disturbances become stable, but the small-scale disturbances, which the surface tension stabilized before, become unstable. This can easily be seen in the linear stability analysis by replacing t by $-t$. Since small-scale disturbances are always introduced by the grid, difficulties are unavoidable. Working on the hypothesis that the large-scale structure is not heavily affected by the surface tension, we ran the code backwards but changed the sign of B, such that the small scales were still stabilized. The relaxation of the mixed layer that we computed in this way was close to being the reverse of its initial growth, but, since the surface tension added to the stabilization, it relaxed a bit more quickly than it had grown. A small disagreement in interface geometry observed during 'forward' and 'backward' evolution could also be attributed to the effect of surface tension.† The width of the mixed layer used for this calculation was roughly five times the wavelength of the most unstable disturbance when we reversed the calculation. The interface was of the type shown later in figure 3(*a*) (but not quite as advanced in evolution).

The effect of resolution was considered by running the same initial configuration on both a 64^2 grid and a 256^2 grid. The shape of the interface and quantitative measures collected were compared at large amplitude and were found to be in close agreement. The interface on the larger grid (four times better resolved) was, however, observed to develop a little faster. This is as one would expect: a poor resolution causes an 'apparent' surface tension that has a stabilizing effect. In most of the runs performed here we have chosen the surface-tension coefficient B large enough so that subgrid scales are damped, yet so small that one must expect the grid effect to slow the evolution a little. There is a trade-off between accuracy and the range of scales that one can simulate. The justification lies in the observation just made, that, although the evolution may be slowed a bit, the same (and, hence, presumably correct) behaviour will be observed. In this sense we claim that the results presented here have been checked for 'convergence'.

The appearance of occasional high-wavenumber waves on the interface, common to many vortex sheet simulations (cf. Baker *et al.* 1982) was observed in runs for $A = 1$ (figure 7). These waves, which appear on the sides of the fingers, have wavelengths equal to approximately two grid spacings, the smallest resolvable wavelength in our simulations. They never reach large amplitudes and usually do not persist for many time steps. Since they do not seem to influence the evolution of the large-scale structure, it was decided that no artificial smoothing would be necessary. However, for interfaces with high surface tension that are compressed strongly, such as the rear of a circular bubble or the tip of a retracting finger, we have encountered

† The rates of relaxation due to gravitational stability and to surface tension are quite different. Straightforward dimensional analysis shows that the width of the mixed layer should decrease proportionally to t for a gravitationally stable interface, but as $t^{-\frac{1}{3}}$ when surface tension is the only driving force.

disturbances that apparently can grow to large amplitude. In the simulations presented here the interface is constantly being stretched, and such phenomena are not observed. We hope to obtain a better understanding of the issues mentioned here as we gain experience with this type of code.

In conclusion we wish to emphasize that, although vortex methods based on direct summation to produce the values of the boundary integrals can probably be made more accurate (by using a higher-order integration formula) than the scheme we are pursuing, they are subject to the $O(N^2)$ operation count problem. And although this operation count is much better than earlier implementations of boundary integral techniques (Baker *et al.* 1980, 1982) it still seems to preclude various flow regimes of considerable physical interest.

3. Numerical results

3.1. *Qualitative observations*

In order to investigate the effect on the evolution of the interface of varying the viscosity ratio A (equation (17)) a number of runs were performed with 1024 particles on a 64^2 grid. The initial condition, which was the same for each run, consisted of an arbitrary collection of small-amplitude waves of various wavelengths. The surface tension was chosen such that the most-unstable wavelength (according to linear stability theory) was about eight grid spacings. The results are shown in figure 3. In each case we show a 'final' stage of the interface at such a value of the width of the mixed layer that the upper and lower boundaries of the computational box have not yet had any noticeable effect. The initial state in the same plot would simply be a horizontal line across the frame. (Later, in figures 5–7 we show a series of pictures of one interface as it evolves.) In all our pictures essentially 'raw data' is being displayed. The vortex elements have simply been connected consecutively by a polygon line to form the plotted interface. No spline or other interpolation is used.

For small amplitudes (less than one wavelength of the dominant instability, say) there is little visible difference between the different cases. However, as the amplitude of the fingers becomes larger, we see important differences. With no viscosity difference ($A = 0$, figure 3*a*) all the initial fingers grow to large amplitude, although some grow a bit faster than others. The difference in finger length becomes more pronounced as the mixed layer widens. The evolution at very large amplitudes is demonstrated more comprehensively later (see figure 5). An obvious feature of this flow is that it is on average symmetric about the original flat interface position, i.e. on average the fingers of the top fluid penetrate the bottom fluid as much as fingers from the bottom penetrate the top. When the viscosity difference is increased, this symmetry is no longer observed (see figures 3*b–f*). The less-viscous fluid penetrates further into the more-viscous one, and the less-viscous fingers are more varied in length than the more-viscous fingers. At later times the longest fingers produce a 'bubble' at the end connected to the 'mother' fluid by a long and narrow neck. Figures 3(*a*, *b*) show that this tendency to form bubbles is more pronounced for $A = 0.5$ than for $A = 0$. Also for small A the bubbles are almost circular in shape. As A increases they become more elongated (see also figure 4). It is likely that in some cases these bubbles will eventually detach and propagate into the more-viscous fluid. Although many of the 'necks' seen in our simulations are dynamically inert, breaking of a narrow neck is not allowed by the coding. Bubble detachment could be incorporated in future work, however. (N. J. Zabusky has introduced the term 'topology change' for algorithms that accomplish such tasks.) In accordance with

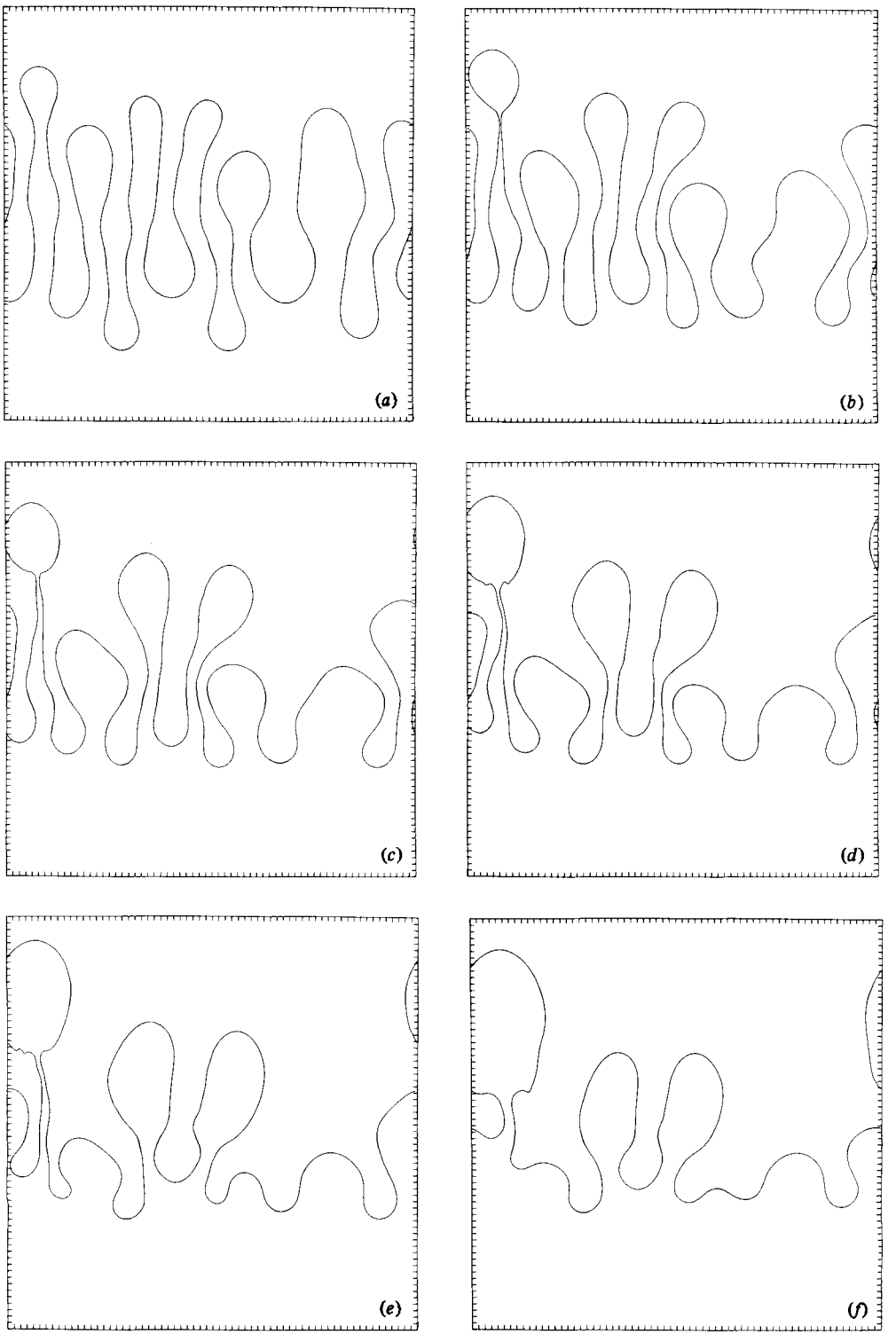

FIGURE 3. Advanced stage of interface evolution for calculations on a 64^2 grid using 1024 vortex elements. Parameter $B = 2 \times 10^{-4}$ for all panels and (*a*) $A = 0$; (*b*) 0.5; (*c*) 0.75; (*d*) 0.85; (*e*) 0.95; (*f*) 1. The initial condition was the same for all values of A.

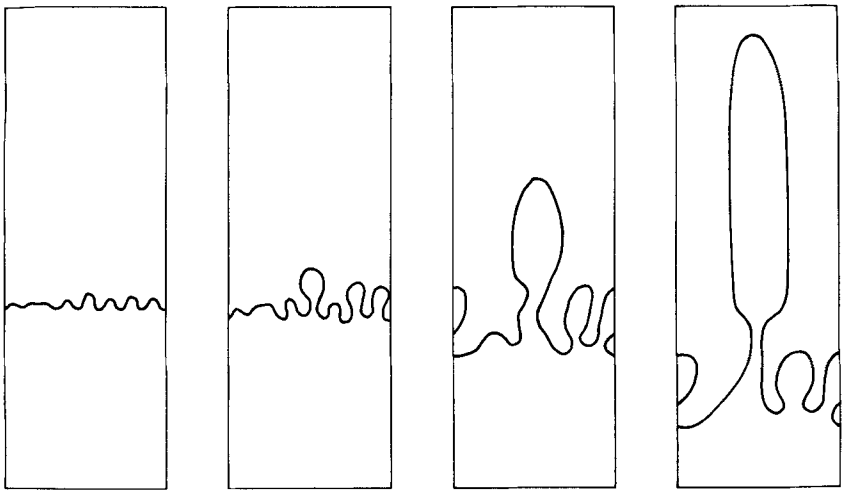

FIGURE 4. The emergence of a single long finger on an interface with $A = 1$ as in the Saffman–Taylor experiment. The width of the computational box is 64 grid spaces and $B = 2 \times 10^{-4}$.

the asymmetry mentioned above, this formation of necks and bubbles is most pronounced on one side of the mixed layer when $A > 0$. As A approaches unity the bubbles become larger.

The smallest fingers in figures 3(*d–f*) reach finite amplitude, but then diminish as larger fingers take over. Hence, in the final state in figs 3(*d–f*) the smallest fingers are much shorter than the small fingers in figures 3(*a–c*), whereas the longest fingers are of comparable length in all pictures. It is worth observing that for A close to unity there seem to be large changes in the interface configuration for small changes in A (for a fixed initial condition). Compare figures 3(*a*, *b*) with figures 3(*e*,*f*). There is as far as we can see no obvious mathematical explanation based on (16) of this sensitivity as A approaches unity. It may be mentioned, however, that the case $A = 1$ corresponds to one of the fluids having essentially zero viscosity, and this is not physically consistent with the derivation of the Hele Shaw equations, which rests upon the condition that both fluids are viscous. Physically, if one of the fluids were inviscid, one should use the Euler equation to describe its motion.

We know of no experimental investigation of the Taylor–Saffman instability for a gravitationally unstable interface between immiscible fluids of similar viscosity. However, even though there is no diffusion through the interface in the model considered here, the results show strong similarities to the miscible-fluid experiment of Wooding (1969) (compare figure 3(*a*), and also figure 5, with Wooding's figure 2). The growth of many fingers to large amplitude and the up–down symmetry of the mixed layer are the predominant features both in Wooding's experiment and in our simulations for the case of no viscosity contrast. We also see how at later stages some fingers overtake others, and thus the number of long fingers is decreased (this is discussed in more detail later). The small fingers do not disappear in our simulations, but in the miscible fluids experiment they do diffuse away.

The run for $A = 1.0$ (figure 3*f*) was rerun in a longer computational box to large amplitude. Results are shown in figure 4 for four stages of the evolution. The first two precede figure 3(*f*) in time, the last two succeed it. (The longest finger has been shifted to the middle of the box for the display in figure 4.) The continued evolution of the interface is now very reminiscent of the Saffman & Taylor (1958) experiment.

First we see growth of initial disturbances whose dominant wavelength is determined by surface tension and is well predicted by linear stability theory (§2). In later stages fewer (highly nonlinear) fingers take over, and the final stage consists primarily of one finger that propagates without much change in shape. In the last two stages shown in figure 4 there are also two small fingers whose amplitudes remain essentially unchanged while the large, dominant finger doubles in length. We assume that the small fingers will eventually go away. This reduction from (in this case) eight initial waves to a single finger is in good qualitative agreement with experiments on immiscible fluids with a large viscosity difference.

There is a celebrated conjecture (Saffman & Taylor 1958; McLean & Saffman 1981) for this type of flow – namely that the width of the propagating finger should be exactly one-half the channel width for sufficiently low surface tension (and should increase with increasing surface tension). Our finger is thinner than half the width of the cell. It is difficult to draw any conclusions from this.† The analytical, single-finger solutions are unstable (McLean & Saffman 1981) so that it is not clear that they should appear at all in an initial-value calculation. The fact that something very similar is seen experimentally may suggest that the appearance of long single fingers occupying half the channel depends, subtly, on effects not explicitly present in the Hele Shaw equations. The fact that we have periodic boundary conditions along the sides instead of the somewhat ill-defined rigid boundaries of the experiments may be significant. Additional comments may be found in §4. Similar remarks can be made for the periodic array of fingers found by Saffman (1959). Note, incidentally, that these are up–down symmetric solutions with $A = 1$. They would definitely not emerge in initial-value calculations of the type reported here.

Runs on a 64^2 grid are too small for any meaningful averaging to be done. We therefore performed additional simulations using 8192 particles on a 256^2 grid. Again the surface tension was chosen in such a way that grid-related effects should be relatively small. Figures 5–7 show the evolution of initially flat interfaces perturbed by an irregular multiwavelength disturbance of very small amplitude. Only that portion of the computational domain containing the interface is shown. The full domain is as wide as it is long. The runs all had the same initial conditions but different viscosity ratios A. As observed for the runs on the 64^2 grid, there is not much difference for small, but still highly nonlinear, amplitudes (compare figures 5*a*, 6*a* and 7*a*). The general behaviour seen in the runs made on a smaller grid is again observed: increasing asymmetry with increasing A, and bubbles on the finger ends that are smallest for A equal to zero. Fewer and fewer fingers grow to large amplitude as A approaches unity. However, we now also observe other phenomena, notably the merging of fingers and finger splitting. These are true 'collective effects' that require a numerical scheme capable of following many fingers simultaneously.

For a typical merging follow the evolution of the first and second finger from the right in figure 6. By the time the interface has evolved to the stage shown in the third panel (figure 6*c*), these fingers have merged. Notice that merging always takes place between fingers of unequal length. The shorter finger is drawn into the bubble at the end of the longer finger from below. Splitting (bifurcation) may also be seen in figure 6. Follow the evolution of the short and wide finger (tenth from the left). Note that when two fingers merge in our simulations the portion of the interface

† G. R. Baker (private communication) has recently produced a single finger of one-half the channel width using similar numerical techniques with zero surface tension. However, Baker's initial conditions contained just one mode of the 'right' wavelength. There was no wavenumber selection as in figure 4.

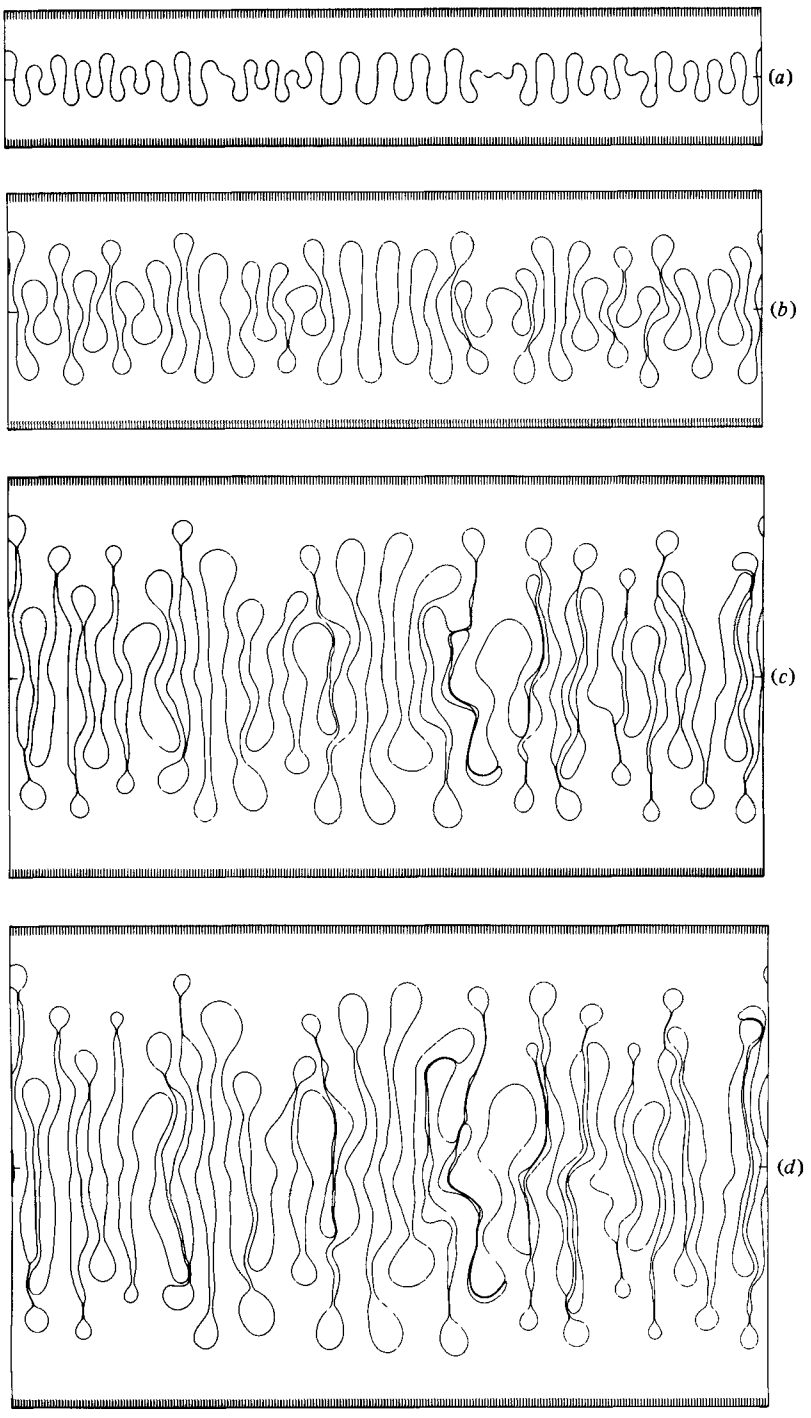

FIGURE 5. Stages in the evolution of an unsteady interface. The initial condition consisted of an arbitrary collection of large-wavenumber waves. $B = 1.25 \times 10^{-5}$ and $A = 0$. Only the portion of the computational box containing the interface is shown. Note the up–down symmetry of the mixed layer and how some fingers grow at the expense of others.

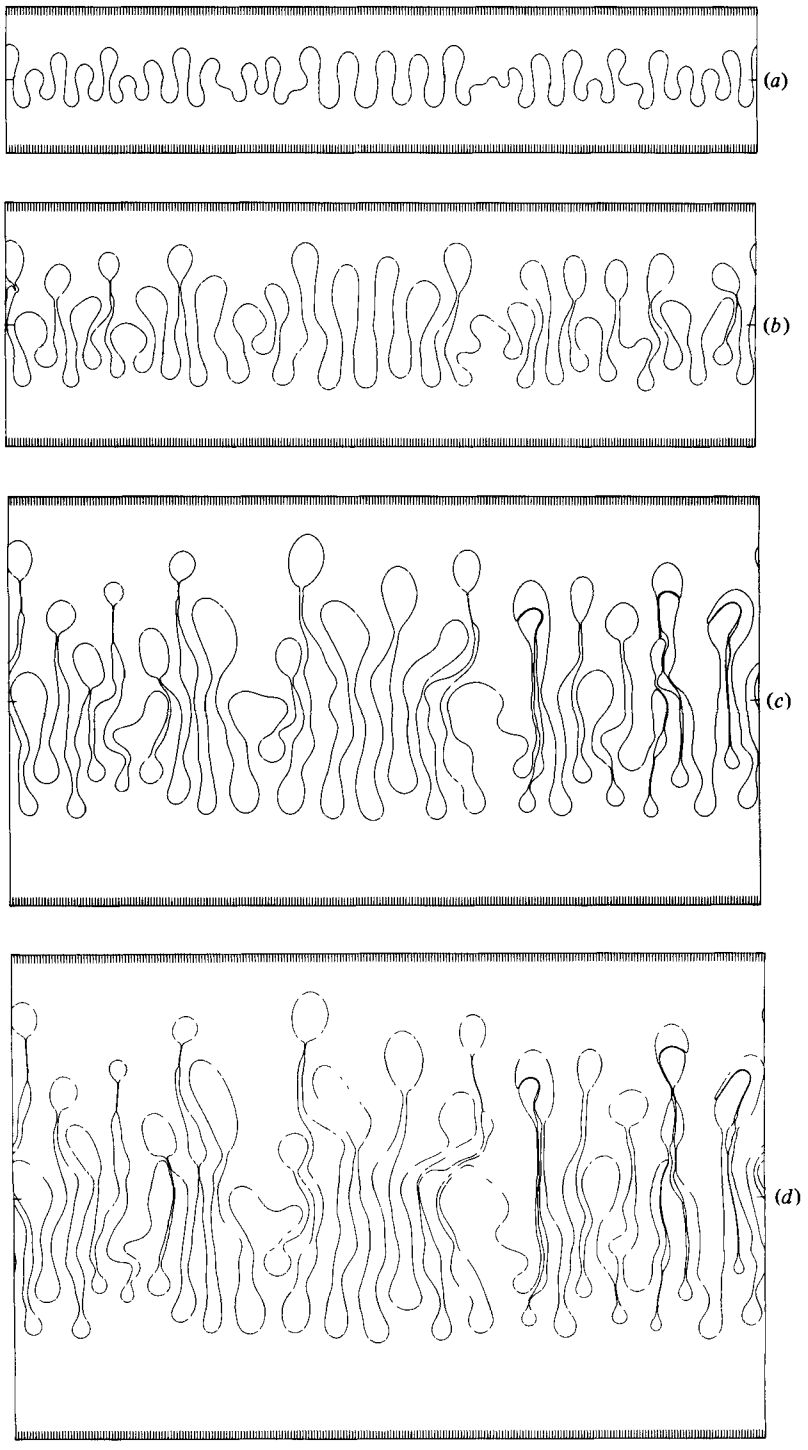

FIGURE 6. Same initial condition (and value of B) as in fig. 5 but $A = 0.5$. The up–down symmetry is destroyed. The amplitudes of fingers of the less-viscous fluid are strongly modulated. The bubbles on the finger tips are larger than for $A = 0$. The bubbles are still almost circular. Note finger merging and splitting.

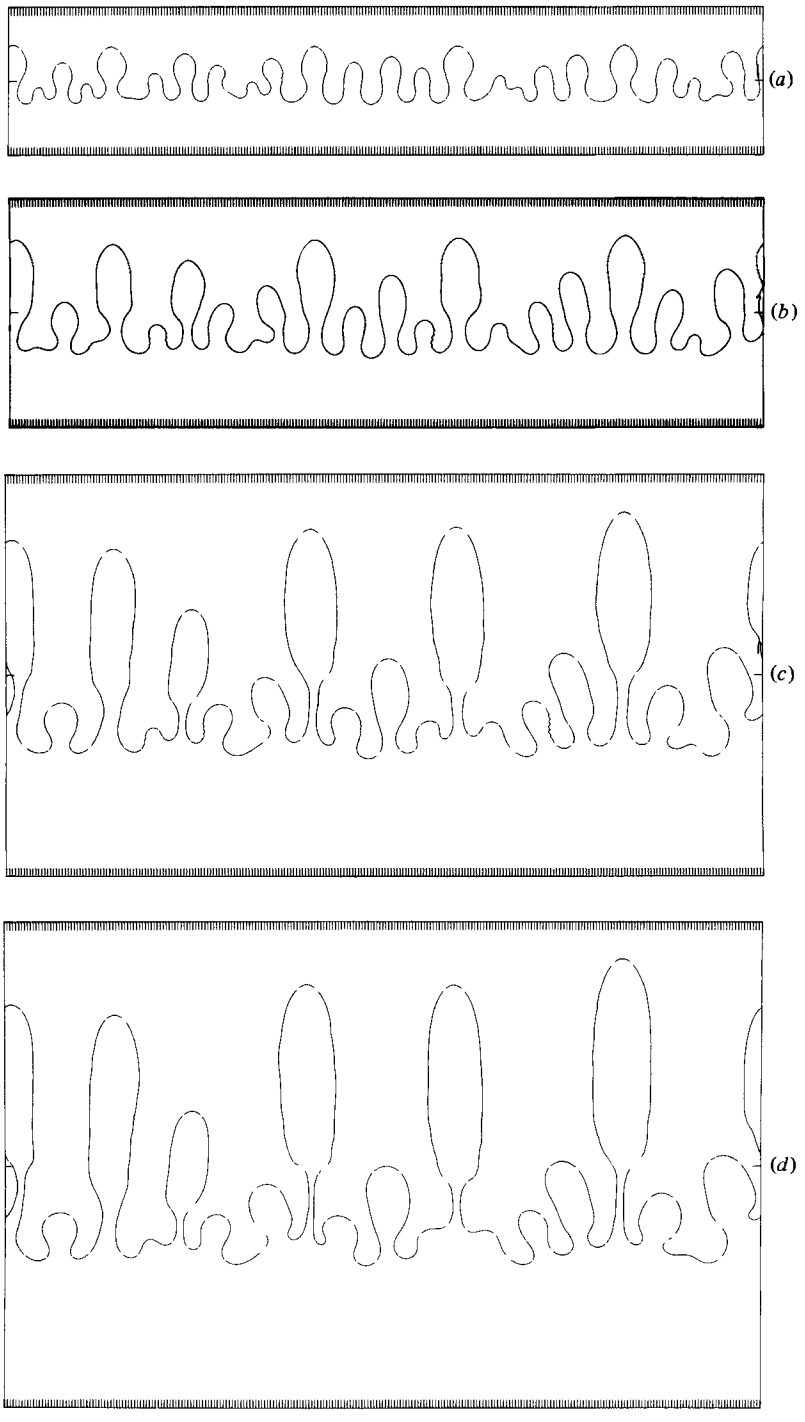

FIGURE 7. Same initial condition (and value of B) as in figures 5 and 6 but $A = 1$. Only a few fingers grow to large amplitude; the rest diminish. The fingers are streamlined in shape, and neither merging nor splitting is observed. The large wavenumber undulations on the sides of some short fingers are numerical artifacts of uncertain origin.

consisting of their common boundary is carried on in the calculation. In principle a 'topology-change' algorithm should be invoked here to erase this double-layered boundary. However, as with the very thin necks attached to the bubbles, we have not implemented such an algorithm at this time. Indeed, we have felt that the good representation of these boundaries is an indication of the physical soundness of the simulations. The application of a 'topology-change' algorithm would, of course, change the geometry of the interface by more than just removing double-layered boundaries. The spike left behind would quickly be pulled back by surface-tension forces, leaving a somewhat shorter finger. The numerical modelling of this breaking of narrow necks implies modelling of molecular-scale phenomena and the criteria for breaking are undoubtedly highly material dependent.

Merging seems to be much more common than splitting, and is one element in the reduction in the number of fingers observed at large amplitude. However, most of the reduction seems to be due to a different process, which is discussed below. In the run with no viscosity difference ($A = 0$) merging takes place on both sides of the mixed layer, but for non-zero A merging only occurs between fingers of the less-viscous fluid. We also observed that splitting mainly occurs for fingers of the less-viscous fluid. Note that we do not observe any splitting of the finger tips as in the experiment of Wooding (1969). In our simulations splitting occurs in the middle of the mixed layer, that is, the fingers that split are not growing very rapidly in length. Some splitting also seems to occur when a long and narrow finger develops a 'kink', which then starts to grow parallel to the original finger (see e.g. the thirteenth finger from the right in figure 5). We suspect that the splitting of finger tips seen in Wooding's experiment is in part due to the interdiffusion of the two fluids used.

The process through which the growth of some fingers is reduced seems to be as follows: if, through a perturbation, a finger becomes shorter than its neighbours, this difference in length increases and it never catches up with them again. This reduction in growth rate of short fingers takes place on both sides of the mixed layer when there is no viscosity difference ($A = 0$). For non-zero A there seems to be a similar reduction in growth rate among the fingers of the less-viscous fluid, but the effect seems much less pronounced among the fingers of the more-viscous fluid.

3.2. *Statistical properties and scaling*

For flow with complicated small-scale structure like the fingering problem, we are obviously mostly interested in averaged quantities. Apart from being too complicated to allow an exact description, it is usually also unnecessary to know the motion of each individual finger. A statistical description of the motion of the interface includes the width of the mixed layer and profiles of various averaged quantities, such as viscosity, density and the mass flux of each fluid. As an indication of the 'degree of mixing' the stretching of the interface is also required. For interfaces with inter-diffusion or chemical reaction the degree of stretching is one of the most important quantities.

By an average of field quantity $f(x, y, t)$ we shall mean a spatial average in x for fixed y and t, viz

$$\langle f \rangle = \frac{1}{W} \int_0^W f(x, y, t)\, \mathrm{d}x, \tag{22}$$

where W is the width of the computational box. Clearly $\langle f \rangle$ depends on y and t. The averages of quantities such as the viscosity or the density that are constant within each fluid can be written as

$$\langle a \rangle = I_1 a_1 + I_2 a_2, \tag{23}$$

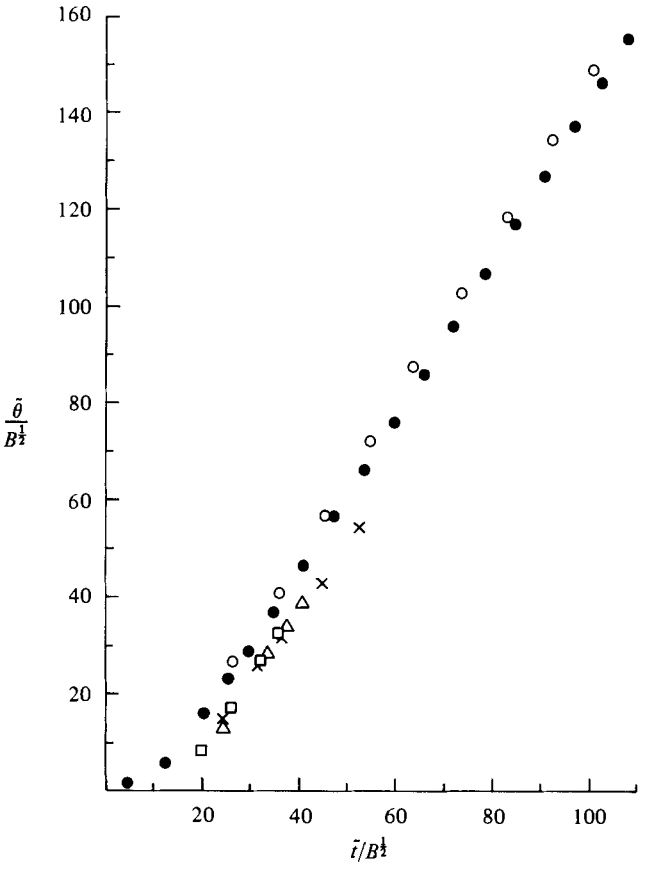

FIGURE 8. The width of the mixed layer *vs.* time for $A = 0$ and several values of the surface tension B. Width and time are scaled as described in §2.1. The symbols correspond to the following values of B: ●, 1.25×10^{-5}; ○, 1.25×10^{-5} (different initial conditions); ×, 2×10^{-4}; △, 4×10^{-4}; □, 6×10^{-4}.

where a_1, a_2 are the two constant values of quantity a, and $I_j(y)$ is the average of a function $i_j(x, y)$ defined as

$$i_j(x,y) = \begin{cases} 1 & \text{inside fluid } j, \\ 0 & \text{otherwise.} \end{cases} \tag{24}$$

Obviously $I_1 + I_2 = 1$. The function $I_1(y)$ is therefore sufficient to determine the profiles for averaged material properties. The average mass flux of each fluid can also be determined from I_1 by the one-dimensional continuity equation. However, I_1 cannot determine the degree of stretching of the interface.

In §2 we derived the appropriate scaling for the evolution of the interface when the only important lengthscale is the one determined by the surface tension. In figures 8 and 9 we check this scaling. Figure 8 shows $\theta' = \tilde{\theta}/B^{\frac{1}{2}}$ versus $t' = \tilde{t}/B^{\frac{1}{2}}$ for several values of B, A equal to zero, and various initial conditions. Here $\theta = \tilde{\theta}W$ is the width of the mixed layer, taken simply as the distance between the tips of those two fingers that have propagated farthest into the upper and lower fluid. Although there is some scatter at early times due to differences in initial conditions, and differing resolutions, it seems fairly safe to conclude that our scaling (§2) is indeed correct. The growth rate goes to a constant independent of B. The growth rate depends on A and on U_* (equation (15)) since, in terms of physical variables, if $\theta' \sim t'$, then $\theta \sim U_* t$ (see §2).

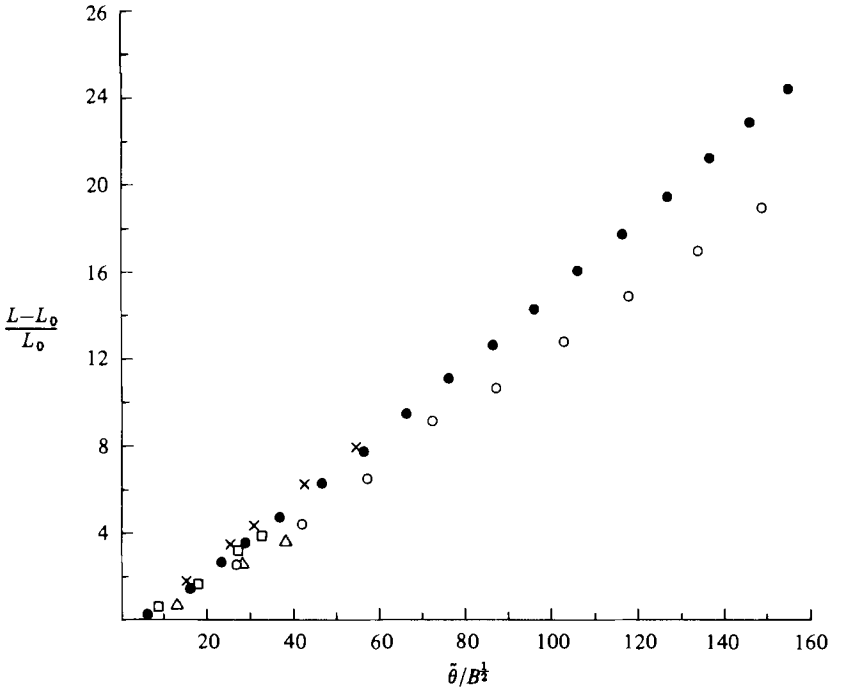

FIGURE 9. Relative stretching of the interface *vs.* width (scaled with $B^{\frac{1}{2}}$) for $A = 0$ and several values of B. The run represented by open dots initially had fewer fingers than the one represented by solid dots. The symbols correspond to the runs in figure 8.

The thickness of the mixed layer gives rather limited information about the structure of the interface. In figure 9 we have plotted the stretching of the interface $(L-L_0)/L_0$ versus the non-dimensional width $\theta' = \tilde{\theta}/B^{\frac{1}{2}}$, also for A equal to zero. Here L is the length of the interface at width θ, and L_0 is the initial length. The scaling is not nearly as good. However, we note that particularly at large amplitudes, where several finger mergings have occurred, the true reduction in interface length due to merging is not represented by the code, since we have not removed double-layered portions of the interface. The run denoted by open circles in figure 9 initially had fewer fingers than the one denoted by solid dots, and, since mergings took place in the latter but not in the former, the total physical lengths are probably closer than the graph indicates.

Having shown that in the regime we are considering the surface tension can be scaled out, we proceed to investigate the effect of A. In figure 10 we have plotted the width θ' versus time t' for different values of A but the same B, and the same initial conditions. The growth rate shows only a weak dependence on A, except for A close to unity, where it is larger. It was checked explicitly that this difference in growth rate is not due to the fact that the fingers for $A = 1$ are bigger, and therefore better resolved, by running similarly resolved fingers for $A = 0$ and $A = 1$.

In order to achieve an analytical estimate of the rate of growth of the mixed layer, let us assume that it can be obtained from the velocity of a bubble of fluid 1 moving in fluid 2 and the velocity of a bubble of fluid 2 moving in fluid 1. It can be shown (Taylor & Saffman 1959, §5) that a circular bubble in unbounded flow will rise (or fall) with speed U_*, so we have $\mathrm{d}\theta'/\mathrm{d}t' = 2$, in our non-dimensional variables, independent of A. This is close to the growth rate that we compute for $A = 0$ and

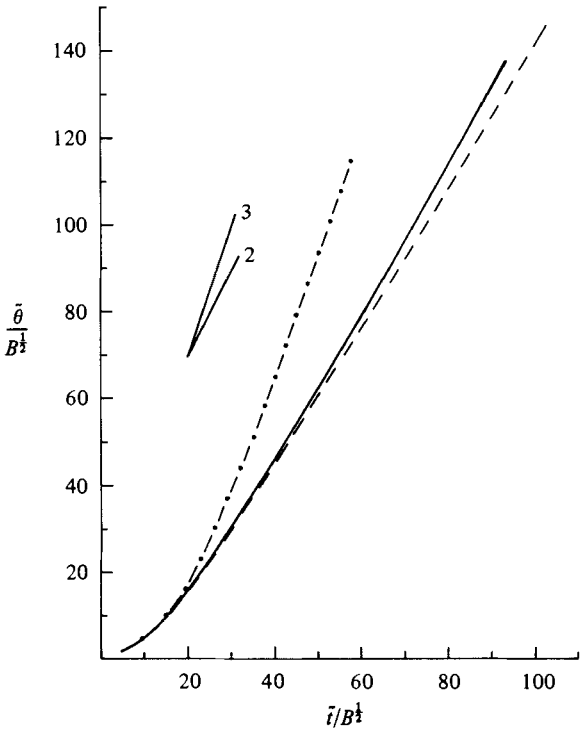

FIGURE 10. The width of the interface *vs.* time (both scaled by $B^{\frac{1}{2}}$) for $B = 1.25 \times 10^{-5}$ and three values of A: ---, 0; ——, 0.5; ·····, 1.

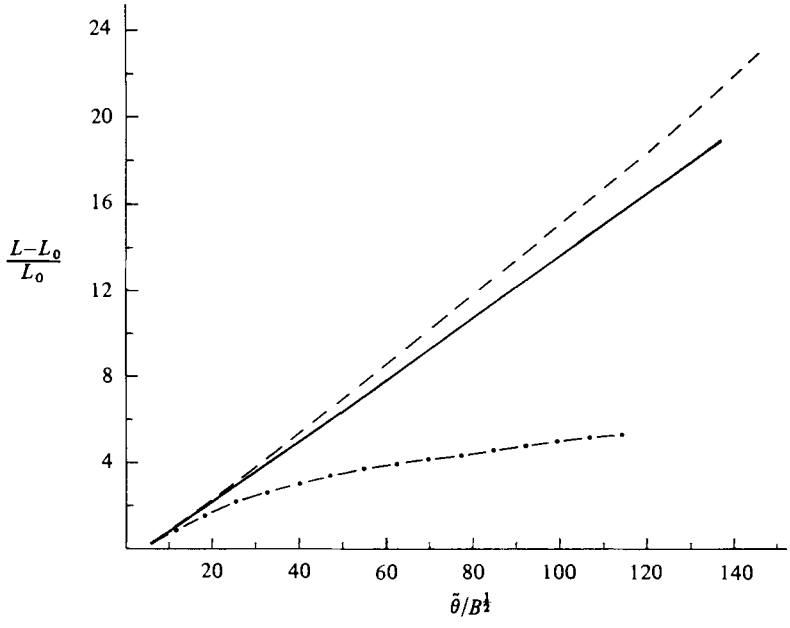

FIGURE 11. Relative stretching of the interface *vs.* width (scaled by $B^{\frac{1}{2}}$) for $B = 1.25 \times 10^{-5}$. Line patterns correspond to the runs in figure 10.

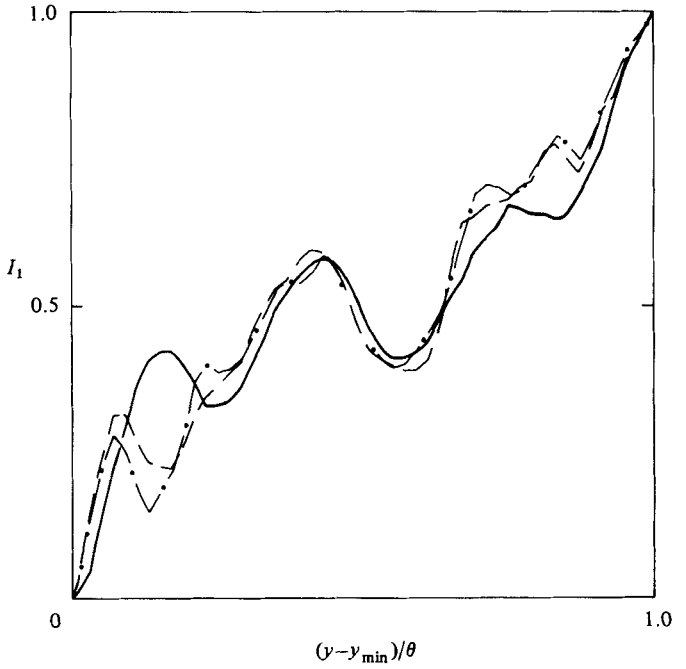

FIGURE 12. Check of scaling prediction (25) for $I(y, t)$; $B = 1.25 \times 10^{-5}$ and $A = 0$: ——, figure 5(*b*); – – –, 5(*c*); —·—, 5(*d*).

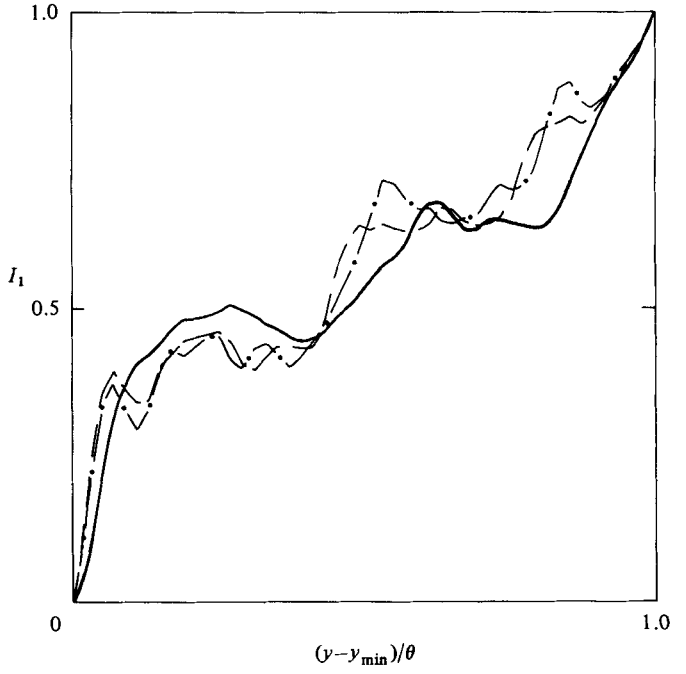

FIGURE 13. Check of scaling prediction (25) for $I(y, t)$; $B = 1.25 \times 10^{-5}$ and $A = 0.5$: ——, figure 6(*b*); – – –, 6(*c*); —·—, 6(*d*).

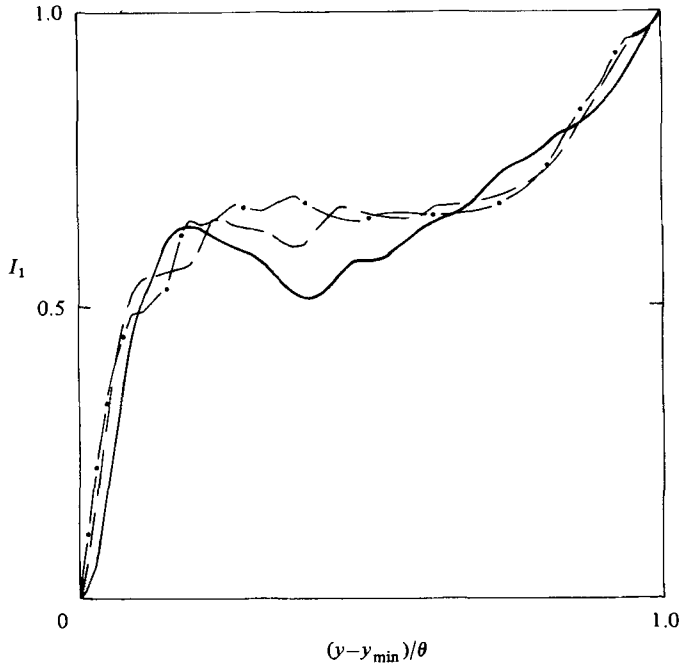

FIGURE 14. Check of scaling prediction (25) for $I(y, t)$; $B = 1.25 \times 10^{-5}$ and $A = 1$: ——, figure 7(*b*); – – –, 7(*c*); —·—, 7(*d*).

$A = 0.5$, where there is indeed a formation of nearly circular bubbles on the fingertips. The reason that the growth rate is considerably higher for $A = 1$ is probably related to the different (more 'streamlined') shape of the fingers. This is in agreement with Taylor & Saffman's (1959) result that the velocity of a bubble increases as it becomes longer and thinner.

In figure 11 we have plotted the stretching of the interface versus the width for the same runs as in figure 10. Again the A-dependence is strongest for A close to unity. This dependence on A is easily understood from the pictures of the development of the interface. The total length of the interface divided by twice the width of the mixed layer can be thought of, roughly, as the mean number of fingers. As shown above the width grows linearly with time, independent of the surface tension and only weakly dependent on A. So, if all fingers grow equally, there is no reduction in the mean number of fingers, and the total length of the interface must grow linearly with the thickness. If there is a reduction in the mean number of fingers, either because some fingers stop growing or because of merging, then the growth rate of the total length is slowed down. Where the reduction in number of fingers is strong, then the deflection from linear growth must be large, and this is indeed observed for A close to unity. Notice that, if the interface developed in such a way that its 'small-scale structure' (i.e. number of fingers) scaled with the width, then the interface length would not increase in figure 11. From our simulations it is clear that this is not so.

Even though the detailed small-scale structure does not scale with the width of the mixed layer, it is quite possible that averaged quantities do. In figures 12–14 we show the mean density profile I_1 (see (23)), scaled with the width of the mixed layer. We are testing the assumption

$$I_1(y, t) = f((y - y_{\min})/\theta; A), \tag{25}$$

where $y_{\min}$ is the smallest y-coordinate of points on the interface. Since A is expected to have a significant effect on I_1, we have plotted I_1 separately for $A = 0$, $A = 0.5$ and $A = 1$. From the figures it seems reasonable to assume that the mean-density profile does indeed scale with the width of the mixed layer. The mean value of I_1 can be interpreted as a measure of the average, relative finger width. Since it is a ratio of two lengths, it must be independent of B, the surface-tension parameter. There seems to be a slight dependence on A, with the average, relative width of the fingers of the less viscous fluid decreasing as A increases.

Since the difference in viscosity causes the growth of fingers to be impeded more on one side of the interface than on the other, as we have discussed, we expect a steep 'mean-density profile' on the side where all fingers grow equally (the less-viscous-fluid side). On the more-viscous-fluid side of the interface, where the lengths of the fingers are more unequal, we expect a more gradual change of the x-averaged density. For $A = 0$ the profile is symmetric, in the sense that the curve in figure 12 looks the same if turned upside down, and we cannot distinguish between the two sides of the mixed layer. For $A = 0.5$ (figure 13) the density profile is already quite asymmetric, and for $A = 1$ (figure 14) the difference between the less-viscous and the more-viscous sides is immediately apparent. A remarkable feature in the profile for $A = 0$ (figure 12) is the 'bump' in the middle. By looking at the corresponding pictures for the evolution of the interface (figure 5) we see that this 'bump' is due to the bubbles at the ends of the fingers.

4. Discussion and conclusions

Traditionally studies of the Taylor–Saffman instability have been concerned with the shape of a single long finger in a channel. Our investigations, on the other hand, have focused on the flow regime where boundary effects are negligible. We have derived the appropriate non-dimensional form of the equations, containing two parameters: A, the Atwood ratio of the viscosities, and B, the surface-tension coefficient non-dimensionalized by other flow parameters. For small-enough B we showed that the equations can be rescaled so that B does not appear explicitly and the only parameter is A. Our numerical simulations of the evolution of an interface show a strong dependency on A. This dependency on the viscosity ratio manifests itself mainly in the way that the fingers interact with one another, rather than in the precise shape of individual fingers. The wavenumber of the most-unstable wave on a flat interface is independent of the viscosity ratio A, but the number of disturbances that grow to highly nonlinear amplitudes depends very strongly on this parameter. The general observation is that by varying A the number of fingers of the less-viscous fluid that penetrate into the more-viscous fluid can be significantly reduced, but the number of fingers of the more-viscous fluid that penetrate into the less-viscous fluid is not affected strongly. Finally, we believe we have observed a subtle secondary 'instability' in the flow regime where one has several competing fingers of finite amplitude.

Investigating the possibility of simple scaling, we find that the average 'density profile' does seem to scale with the width of the mixed layer, but, as far as the small-scale structure is concerned (that is, the number and shape of fingers), scaling is much less certain. A simple scaling assumption is that the interface geometry can be described by a relation of the form

$$\frac{y}{\theta} = F\left(\frac{x}{\theta^{1-\alpha}\xi^{\alpha}}\right) \tag{26}$$

where ξ is a fixed length, e.g. the wavelength of the most-unstable wave (on the initial interface). Here we assume for simplicity that y is a single-valued function of x. This is true during the initial stages of evolution. If $\alpha = 0$ (26) corresponds to a simple stretching of the fingers that appear initially. For $\alpha = 1$ an interface evolving according to (26) would display a sufficiently large reduction in the number of fingers that the interface length would remain constant. From our simulations we may roughly identify $\alpha \sim 0$ with $A = 0$ and $\alpha \sim 1$ with $A = 1$, if the above scaling is valid. However, for $\alpha = 1$ the scaling law (26) describes a reduction in fingers with a mechanism that is quite different from the one actually observed in our simulations. Furthermore, averaged quantities (like I_1) for an interface that develops according to (26) are independent of α, which in turn determines the A-dependency. This is again in contradiction to our numerical results. We have been unable to obtain a scaling form that provides a better description of our simulated interfaces.

The rate of stretching is obviously proportional to the number of growing fingers, and since there is a strong reduction in the number of fingers for $A = 1$, it is not certain that one can expect a constant rate of stretching in that case. If the interface for $A = 1$ continues to develop fewer and larger fingers, it must eventually feel the presence of external boundaries, and then the scaling of §2.1 ceases to be valid. If this is the case, there is no asymptotic state for $A = 1$ in the many-finger flow regime, and we are only observing transient development. However, for very wide fingers secondary Taylor–Saffman instability might be possible at the finger tips. In order to observe that, a considerably lower surface tension (or a bigger finger) than obtained in our simulations is necessary.

The equations considered in this paper omit several complications that must be faced in applications. The two most obvious additions to the primitive Hele Shaw equations are interdiffusion and, in the context of the Darcy law, variable saturation. Both of these effects are not easily handled by a code of the type used here. The problem of variable saturation has been studied by Glimm, Marchesin & McBryan (1980). They use a moving finite-element code coupled with the so-called random-choice method. For the interdiffusion problem it is also likely that some form of a moving grid is necessary.

In the derivation of our model equations two essential simplifications of the boundary conditions at the interface have been made. First, we have completely neglected the three-dimensionality of the flow there. It is difficult to estimate the influence of this simplification, but it seems reasonable to assume that the modification of the flow is less than at a rigid boundary. In any case, this is a complication that is not accessible to our numerical method. The second simplification of the interfacial conditions is the assumption of constant wetting angle. The effect of this assumption is probably most serious for large viscosity difference and a very small gap between the plates. It is observed experimentally that the contact angle for an advancing interface (say air replacing oil) is smaller than for a retreating one. The determination of this angle is a non-trivial problem and far from being completely solved (see the review by Dussan V. 1979). However, given the contact angle as a function of the velocity, this effect can easily be incorporated into our code. A velocity-dependent pressure drop across the interface will introduce a third non-dimensional coefficient into the problem (in addition to A and B) and it will no longer be true that a gravitationally unstable Hele Shaw cell is equivalent to a velocity-driven one. We intend to perform a quantitative study of this effect by assuming simple forms for the pressure drop function. Additional complications arise when one fluid, as it is replaced by the other, leaves a film on the glass plates. If this film is of constant

thickness, its effect is easily taken into account (McLean & Saffman 1981). However, such a film may not have constant thickness.

If the change in material properties is gradual, and not abrupt, we can model the flow using many interfaces as long as the properties of each material point are approximately constant. That is, diffusion must be much slower than the velocities of the interfaces. Variable surface tension along the interface(s) can also be handled. Finally, our code can be modified to accommodate potential flows different from the simple uniform flow used here. Studies of some of these extensions are already under way and will be reported in future publications.

One of us (G.T.) would like to thank the Graduate School at Brown University for fellowship support during the initial stages of the research reported here. This work was supported by National Science Foundation grant MEA 81-16910 to Brown University. We should like to thank the group in Mechanics within the Division of Engineering at Brown for allowing us to use their VAX 11/780 facility during phases of code development. We are indebted to the Scientific Computing Division at the National Center for Atmospheric Research for granting us time on their CRAY-1 and CDC 7600 computers. NCAR is sponsored by the NSF.

REFERENCES

AREF, H. 1983 Integrable, chaotic, and turbulent vortex motion in two-dimensional flows. *Ann. Rev. Fluid Mech.* **15**, 345–389.

AREF, H. & SIGGIA, E. D. 1980 Vortex dynamics of the two-dimensional tubulent shear layer. *J. Fluid Mech.* **100**, 705–737.

AREF, H. & SIGGIA, E. D. 1981 Evolution and breakdown of a vortex street in two dimensions. *J. Fluid Mech.* **109**, 435–463.

AREF, H. & TRYGGVASON, G. 1982 Numerical experiments on statistical fingering in stratified Hele Shaw flows. *Bull. Am. Phys. Soc.* **27**, 1172 (abstract only).

AREF, H. & TRYGGVASON, G. 1984 Vortex dynamics of passive and active interfaces. *Physica* D (to appear).

BAKER, G. R., MEIRON, D. I. & ORSZAG, S. A. 1980 Vortex simulation of the Rayleigh–Taylor instability. *Phys. Fluids* **23**, 1485–1490.

BAKER, G. R., MEIRON, D. I. & ORSZAG, S. A. 1982 Generalized vortex methods for free-surface flow problems. *J. Fluid Mech.* **123**, 477–501.

BATCHELOR, G. K. 1967 *An Introduction to Fluid Dynamics.* Cambridge University Press.

BEAR, J. 1972 *Dynamics of Fluids in Porous Media.* Elsevier.

BIRKHOFF, G. 1954 Taylor instability and laminar mixing. *Los Alamos Sci. Lab. Rep.* LA-1862; appendices in *Rep.* LA-1927.

CHUOKE, R. L., VAN MEURS, P. & VAN DER POEL, C. 1959 The instability of slow immiscible, viscous liquid–liquid displacements in permeable media. *J. Petrol. Tech.* **11**, 64.

CHRISTIANSEN, J. P. 1973 Numerical simulation of hydrodynamics by the method of point vortices. *J. Comp. Phys.* **13**, 363–379.

DE JOSSELIN DE JONG, G. 1960 Singularity distributions for the analysis of multiple-fluid flow through porous media. *J. Geophys. Res.* **65**, 3739–3758.

DUSSAN V., E. B. 1979 On the spreading of liquids on solid surfaces: static and dynamic contact lines. *Ann. Rev. Fluid Mech.* **11**, 371–400.

GLIMM, J., MARCHESIN, D. & MCBRYAN, O. 1980 Statistical fluid dynamics: unstable fingers. *Commun. Math. Phys.* **74**, 1–13.

GUPTA, S. P., VARNON, J. E. & GREENKORN, R. A. 1973 Viscous finger wavelength degeneration in Hele Shaw models. *Water Resources Res.* **19**, 1039–1046.

HELE SHAW, J. H. S. 1898 The flow of water. *Nature* **58**, 34–36.

LAMB, H. 1932 *Hydrodynamics*, art. 330. Dover.

LANGER, J. S. 1980 Instabilities and pattern formation in crystal growth. *Rev. Mod. Phys.* **52**, 1–28.

LEONARD, A 1980 Vortex methods for flow simulation. *J. Comp. Phys.* **37**, 289–335.

LONGUET-HIGGINS, M. S. & COKELET, E. D. 1976 The deformation of steep surface waves on water. II. Growth of normal-mode instabilities. *Proc. R. Soc. Lond.* A **364**, 1–28.

MCLEAN, J. W. & SAFFMAN, P. G. 1981 The effect of surface tension on the shape of fingers in a Hele Shaw cell. *J. Fluid Mech.* **102**, 455–469.

MENG, J. C. S. & THOMSON, J. A. L. 1978 Numerical studies of some nonlinear hydrodynamic problems by discrete vortex element methods. *J. Fluid Mech.* **84**, 433–453.

MEYER, G. H. 1981 Hele-Shaw flow with a cusping free boundary. *J. Comp. Phys.* **44**, 262–276.

MOORE, D. W. 1981 On the point vortex method. *SIAM J. Sci. Stat. Comp.* **2**, 65–84.

OVERMAN, E. A., ZABUSKY, N. J. & OSSAKOW, S. L. 1983 Ionospheric plasma cloud dynamics via regularized contour dynamics. I. Stability and nonlinear evolution of one-contour models. *Phys. Fluids* **26**, 1139–1153.

PATERSON, L. 1981 Radial fingering in a Hele-Shaw cell. *J. Fluid Mech.* **113**, 513–529.

PERKINS, T. K., JOHNSTON, O. C. & HOFFMAN, R. N. 1965 Mechanics of viscous fingering in miscible systems. *Soc. Petrol. Engng J.* **5**, 301–317.

PITTS, E. 1980 Penetration of fluid into a Hele Shaw cell: the Saffman–Taylor experiment. *J. Fluid Mech.* **97**, 53–64.

POLLARD, D. D., MULLER, O. H. & DOCKSTADER, D. R. 1975 The form and growth of fingered sheet intrusions. *Geol. Soc. Am. Bull.* **86**, 351–363.

PRANDTL, L. & TIETJENS, O. G. 1934 *Fundamentals of Hydro- and Aeromechanics.* Dover.

RICHARDSON, J. G. 1961 Flow through porous media. In *Handbook of Fluid Dynamics* (ed. V. L. Streeter). McGraw-Hill.

RIGELS, F. 1938 Zur Kritik des Hele-Shaw-Versuchs. *Z. angew. Math. Mech.* **18**, 95–106.

ROSENHEAD, L. 1931 The formation of vortices from a surface of discontinuity. *Proc. R. Soc. Lond.* A **134**, 170–192.

ROSENSWEIG, R. E. 1982 Magnetic fluids. *Sci. Am.* **247** (4), 136–145.

SAFFMAN, P. G. 1959 Exact solutions for the growth of fingers from a flat interface between two fluids in a porous medium or Hele-Shaw cell. *Q. J. Mech. Appl. Maths* **12**, 146–150.

SAFFMAN, P. G. & TAYLOR, G. I. 1958 The penetration of a fluid into a porous medium or Hele-Shaw cell containing a more viscous liquid. *Proc. R. Soc. Lond.* A **245**, 312–329.

SHAMPINE, L. F. & GORDON, M. K. 1975 *Computer Solution of Ordinary Differential Equations.* Freeman.

SLOBOD, R. L. & THOMAS, R. A. 1963 Effect of transverse diffusion on fingering in miscible-phase displacement. *Soc. Petrol. Engng J.* **3**, 9–13.

TAYLOR, G. I. & SAFFMAN, P. G. 1959 A note on the motion of bubbles in a Hele-Shaw cell and porous medium. *Q. J. Mech. Appl. Maths* **12**, 265–279.

THOMPSON, B. W. 1968 Secondary flow in a Hele-Shaw cell. *J. Fluid Mech.* **31**, 379–395.

TODD, D. K. 1955 Flow in porous media studied by Hele-Shaw channel. *Civil Engng slab* **25**, 85.

VAN MEURS, P. 1957 The use of transparent three-dimensional models for studying the mechanism of flow processes in oil reservoirs. *Trans. AIME* **210**, 295–301.

WOODING, R. A. 1969 Growth of fingers at an unstable diffusing interface in a porous medium or Hele-Shaw cell. *J. Fluid Mech.* **39**, 477–495.

WOODING, R. A. & MOREL-SEYTOUX, H. J. 1976 Multiphase fluid flow through porous media. *Ann. Rev. Fluid Mech.* **8**, 233–274.